AFRO ASAIN JOURNALS

Satinder Kumar et al, Afro Asian J Sci Tech, 2016,3(1),263-283 ***ISSN 2349-4964***

Deformation due to thermomechanical source in thermoporoelastic medium

Rajneesh Kumar[1], Satinder Kumar[2] and M. G. Gourla[3]

1.Department of Mathematics, Kurukshetra University, Kurukshetra, Haryana, India

2. Department of Mathematics, Govt. Degree College Chowari (Chamba), Himachal Pradesh, India

3. Department of Mathematics, Himachal Pradesh University, Shimla-171005, India

Abstract:

The present investigation deals with the response of thermomechanical sources in a thermoporoelastic medium. Laplace and Fourier transforms are applied to investigate the problem. As an application of the approach concentrated and distributed sources are taken to illustrate the utility of the approach. The expressions for displacement components, stress components, pore pressure and temperature change are obtained in the transformed domain. Numerical inversion technique has been applied to obtain the solution in physical domain. Effect of porosity is shown on the resulting quantities. A particular case of interest is also deduced from the present investigation.

Key words: Thermoporoelastic, Integral transform, sources

Introduction:

Coupled thermal and poro-mechanical processes play an important role in a number of problems of interest in the geomechanics such as stability of bore hole and permeability enhancement in geothermal reservoirs or high temperature petroleum bearing formations. A thermoporoelastic approach combine the theory of heat conduction with poroelastic constitutive equations and coupling the temperature field with the stresses and pore pressure.

Most of the modern engineering structures are generally made up of multiphase porous continuum, the classical theory, which represent a fluid saturated porous medium as a single phase material, is inadequate to represent the mechanical behaviour of such material especially when the pore are filled with liquid. In this context the solid and liquid phases have different motions. Due to these different motions, the different material properties and the complicated geometry of pore structures, the mechanical behaviour of a fluid saturated porous medium is very complex and difficult.

Based on the work of Von Terzaghi [1,2], Biot[3] proposed a general theory of three dimensional deformations of liquid saturated porous solid. Biot[4,5,6] theory is based on the assumption of compressible constituents and till recently, some of his results have taken as standard references and basis for subsequent analysis in acoustic, geophysics and other such fields.

Kumar and Hundal [7] discussed the wave propagation in a fluid saturated incompressible porous medium. Bai and Li [8] found a solution for cylindrical cavity in saturated thermoporoelastic medium by using Laplace transform and numerical Laplace transform inversion. Bai [9] investigated the response of saturated porous media subjected to local thermal loading on the surface of semi space. Bai [10] discussed the thermal response of saturated porous spherical body containing a cavity under several boundary conditions. He also studied the fluctuation responses of porous media subjected to cyclic thermal loading [11].

Kaushal, Kumar and Miglani [12] discussed the response of frequency domain in generalized thermoelasticity with two temperature. Jabbari and Dehbani [13] obtained the exact solution for classic coupled thermoelasticity in axisymmetric cylinder. They also discussed an exact solution for quasi-static poro- thermoelasticity in spherical coordinate[14] . Mixed variation principal for dynamic response of thermoelastic and poroelastic continua was discussed by Apostolakis and Dargus [15]. Hou, et. al. [16] discussed the three dimensional Green's function for transversely isotropic thermoporoelastic biomaterial. Jabbari et.al. [17] also discussed thermal buckling analysis of functionally graded thin circular plate made of saturated porous materials.

Liu and Chain[18]discussed a micromechanical analysis of the fracture properties of saturated porous media. He et al.[19] studied the dynamic simulation of landslide based on thermoporoelastic approach. Nguyen et al.[20] discussed the analytical study of freezing behaviour of a cavity in thermoporoelastic medium. Wu et al. [21] presented a refined theory of axisymmetric thermoporoelastic circular cylinder.

In the present paper, we obtain the components of displacement, stress, pore pressure and temperature change due to concentrated source and distributed source in thermoporoelastic medium. Laplace and Fourier transforms are used to investigate the problem. Numerical inversion technique is applied to obtain the resulting quantities in a physical domain. The resulting quantities are shown graphically to depict the effect of porosity.

Governing Equations

Following Jabbari and Dehbani [22], the basic equations are

$$(\lambda+\mu)\nabla\nabla.\vec{u}+\mu\nabla^2\vec{u}-\alpha\nabla p-\beta\nabla T=\rho\frac{\partial^2\vec{u}}{\partial t^2}\ , \qquad (1)$$

$$\frac{k}{\gamma_w}\nabla^2 p-\alpha_p\dot{p}-Y\dot{T}-\alpha div\dot{\vec{u}}=0\ , \qquad (2)$$

$$K\nabla^2 T-ZT_0\dot{T}+YT_0\dot{p}-\beta T_0 div\dot{\vec{u}}=0\ , \qquad (3)$$

$$\sigma_{ij}=\lambda u_{k,k}\delta_{ij}+\mu\left(u_{i,j}+u_{j,i}\right)-\alpha p\delta_{ij}-\beta T\delta_{ij}\ , \qquad (4)$$

where $\vec{u}$ is the displacement component, p is the pore pressure, ρ is the bulk mass density , $\alpha=1-\frac{C_s}{C}$ is the Biot's coefficient , $C_s=3(1-2v_s)/E_s$ is the coefficient of volumetric compression of solid grain , with E_s and v_s being the elastic modulus and Poisson's ratio of solid grain , $C=3(1-2v)/E$ is the coefficient of volumetric compression of solid skeleton , with E and v being the elastic modulus and Poisson's ratio of solid skeleton , T_0 is initial reference temperature , $\beta=\frac{3\alpha_s}{C}$ is the thermal expansion factor , α_s is the coefficient of linear thermal expansion of solid grain , $Y=3(n\alpha_w+(\alpha-n)\alpha_s)$ and $\alpha_p=n(C_w-C_s)+\alpha C_s$ are coupling parameters , α_w and C_w are the coefficients of linear thermal expansion and volumetric compression of pure water , n is the porosity , k is the hydraulic conductivity , γ_w is the unit of pore water and $Z=\frac{(1-n)\rho_s C_s+n\rho_w C_w}{T_0}$ is coupling parameter , ρ_w and ρ_s are densities of pore water and solid grain and C_w and C_s are heat capacities of pore water and solid grain and K is the coefficient of heat conductivity.

Formulation of the problem

We consider homogeneous thermoporoelastic half space $x_3\geq 0$ of a rectangular Cartesian coordinate system (x_1,x_2,x_3) having origin at the surface $x_3=0$, x_3 – axis pointing vertically downward in the medium. A concentrated and distributed mechanical or thermal source is assumed to be acting at the origin. We restrict our analysis to the plane strain parallel to x_1-x_3 plane. The complete geometry of the problem is shown in Fig.1. So we take displacement vector $\vec{u}$ as

$$\vec{u}=(u_1(x_1,x_3),0,u_3(x_1,x_3)) \qquad (5)$$

Equations(1)-(3)with the aid of (5) ,take the form

$$\mu\nabla^2 u_1+(\lambda+\mu)\frac{\partial e}{\partial x_1}-\alpha\frac{\partial p}{\partial x_1}-\beta\frac{\partial T}{\partial x_1}=\rho\frac{\partial^2 u_1}{\partial t^2}\ , \qquad (6)$$

$$\mu\nabla^2 u_3 + (\lambda+\mu)\frac{\partial e}{\partial x_3} - \alpha\frac{\partial p}{\partial x_3} - \beta\frac{\partial T}{\partial x_3} = \rho\frac{\partial^2 u_3}{\partial t^2} \quad , \tag{7}$$

$$\frac{k}{\gamma_w}\nabla^2 p - \alpha_p\dot{p} - Y\dot{T} - \alpha\frac{\partial e}{\partial t} = 0 \quad , \tag{8}$$

$$K\nabla^2 T - ZT_0\dot{T} + YT_0\dot{p} - \beta T_0\frac{\partial e}{\partial t} = 0. \tag{9}$$

We define the dimensionless quantities

$$x_1' = \frac{\omega^*}{c_1}x_1,\ x_3' = \frac{\omega^*}{c_1}x_3,\ u_1' = \frac{\omega^*\rho c_1}{\beta T_0}u_1,\ u_3' = \frac{\omega^*\rho c_1}{\beta T_0}u_3,\ p' = \frac{p}{\beta T_0},$$

$$c_1^2 = \frac{\lambda+2\mu}{\rho},\ t' = \omega^* t,\ T' = \frac{T}{T_0},\ \omega^* = \frac{ZT_0c_1^2}{K},\ \sigma_{33}' = \frac{\sigma_{33}}{\beta T_0},\ \sigma_{31}' = \frac{\sigma_{31}}{\beta T_0} \tag{10}$$

where ω^* is a constant having the dimensions of frequency.

Using the dimensionless quantities defined by (10) in equations (6)-(9) yield

$$\frac{\partial e}{\partial x_1} + a_1\nabla^2 u_1 - a_2\frac{\partial p}{\partial x_1} - a_3\frac{\partial T}{\partial x_1} = a_4\frac{\partial^2 u_1}{\partial t^2} \quad , \tag{11}$$

$$\frac{\partial e}{\partial x_3} + a_1\nabla^2 u_3 - a_2\frac{\partial p}{\partial x_3} - a_3\frac{\partial T}{\partial x_3} = a_4\frac{\partial^2 u_3}{\partial t^2} \quad , \tag{12}$$

$$b_1\nabla^2 p - b_2\frac{\partial p}{\partial t} - b_3\frac{\partial T}{\partial t} - \frac{\partial e}{\partial t} = 0 \quad , \tag{13}$$

$$b_4\nabla^2 T - b_5\frac{\partial T}{\partial t} + b_6\frac{\partial p}{\partial t} - \frac{\partial e}{\partial t} = 0 \quad , \tag{14}$$

where

$$a_1 = \frac{\mu}{\lambda+\mu},\ a_2 = \frac{\alpha\rho c_1^2}{\lambda+\mu},\ a_3 = \frac{\rho c_1^2}{(\lambda+\mu)},\ a_4 = \frac{\rho c_1^2}{\lambda+\mu},\ b_1 = \frac{k\omega^*\rho}{\gamma_w\alpha},\ b_2 = \frac{\alpha_p\rho c_1^2}{\alpha}$$

$$b_3 = \frac{Y\rho c_1^2}{\alpha},\ b_4 = \frac{K\omega^*\rho}{\beta^2 T_0},\ b_5 = \frac{Z\rho c_1^2}{\beta^2},\ b_6 = \frac{Y\rho c_1^2}{\beta^2},$$

and $e = \frac{\partial u_1}{\partial x_1} + \frac{\partial u_3}{\partial x_3}$.

The displacement components u_1 and u_3 are related to the potential functions $\Phi(x_1, x_3, t)$, $\Psi(x_1, x_3, t)$ as

$$u_1 = \frac{\partial\Phi}{\partial x_1} - \frac{\partial\Psi}{\partial x_3},\ u_3 = \frac{\partial\Phi}{\partial x_3} + \frac{\partial\Psi}{\partial x_1} \tag{15}$$

Equations (11) - (14) with the aid of (15) take the form

$$(1+a_1)\nabla^2\Phi - a_2 p - a_3 T - a_4\frac{\partial^2\Phi}{\partial t^2} = 0 \quad , \tag{16}$$

$$a_1\nabla^2\Psi - a_4\frac{\partial^2\Psi}{\partial t^2} = 0 \quad , \tag{17}$$

$$b_1\nabla^2 p - b_2\frac{\partial p}{\partial t} - b_3\frac{\partial T}{\partial t} - \frac{\partial}{\partial t}[\nabla^2\Phi] = 0 \quad , \tag{18}$$

$$b_4\nabla^2 T - b_5\frac{\partial T}{\partial t} + b_6\frac{\partial p}{\partial t} - \frac{\partial}{\partial t}[\nabla^2\Phi] = 0 \quad . \tag{19}$$

We define the Laplace and Fourier transforms as follows:

$$\bar{f}(s) = \int_0^\infty f(t)e^{-st}\,dt \tag{20}$$

$$\tilde{\bar{f}}(\xi) == \int_{-\infty}^{\infty}\bar{f}(\xi)e^{i\xi x_1}dx \quad . \tag{21}$$

Applying Laplace and Fourier transforms defined by (20) and (21) on equations (16)-(19) and eliminating $\tilde{\bar{p}}$ and $\tilde{\bar{T}}$ from resulting equations, we obtain

$$\left[A_1\frac{d^6}{dx_3^6} + A_2\frac{d^4}{dx_3^4} + A_3\frac{d^2}{dx_3^2} + A_4\right]\tilde{\bar{\Phi}} = 0 \ , \tag{22}$$

$$a_1\left(\frac{d^2}{dx_3^2} - \xi^2\right)\tilde{\bar{\Psi}} - a_4 s^2\tilde{\bar{\Psi}} = 0 \quad , \tag{23}$$

where

$A_1 = b_1 b_4 (1 + a_1)$, $A_2 = -3\xi^2 b_1 b_4 (1 + a_1) - s(1 + a_1)(b_1 b_5 + b_2 b_4) - a_4 b_1 b_4 s^2 - a_2 b_4 s - a_3 b_1 s$,

$A_3 = 3\xi^4 b_1 b_4 (1 + a_1) + 2\xi^2 s(1 + a_1)(b_1 b_5 + b_2 b_4) + s^2(1 + a_1)(b_1 b_5 + b_2 b_4) + 2\xi^2 s^2 a_4 b_1 b_4 + a_4 s^3 (b_1 b_5 + b_2 b_4) + 2\xi^2 a_2 b_4 s - a_2 s^2 (b_3 - b_5) + 2\xi^2 a_3 b_1 s + a_3 s^2 (b_6 + b_2)$

$A_4 = -\xi^6 b_1 b_4 (1 + a_1) - s\xi^4 (1 + a_1)(b_1 b_5 + b_2 b_4) + s^2 \xi^2 (1 + a_1)(b_1 b_5 + b_2 b_4) - a_4 b_1 b_4 s^2 \xi^4 - a_4 s^3 \xi^2 (b_1 b_5 + b_2 b_4) - a_4 s^4 (b_2 b_5 + b_3 b_6) - a_2 b_4 s\, \xi^4 + a_2 s^2 (b_3 - b_5)\xi^2 - \xi^4 a_3 b_1 s - a_3 s^2 \xi^2 (b_6 + b_2)$.

Solving (22) and (23) and assuming that $\tilde{\bar{\Phi}}, \tilde{\bar{\Psi}}$,$\tilde{\bar{p}}$ and $\tilde{\bar{T}} \to$0 as $x_3 \to \infty$ we obtain the value of $\tilde{\bar{\Phi}}, \tilde{\bar{\Psi}}$, $\tilde{\bar{p}}$ and $\tilde{\bar{T}}$as $(\tilde{\bar{\Phi}}, \tilde{\bar{p}}\ \tilde{\bar{T}}) = \sum_{i=1}^{3} (1, r_i, s_i)\, B_i e^{-m_i x_3}$ (24)

$\tilde{\bar{\Psi}} = B_4 e^{-m_4 x_3}$ (25)

where m_1, m_2, m_3 are the roots of the equation (22) and

$m_4 = \sqrt{A_5}$

where $A_5 = \xi^2 + \frac{a_4}{a_1} s^2$

and the coupling constants are given by

$$r_i = \frac{b_4 s\left(m_i^2 - \xi^2\right)^2 + \left(b_3 s^2 - b_5 s^2\right)\left(m_i^2 - \xi^2\right)}{b_1 b_4 \left(m_i^2 - \xi^2\right)^2 - \left(b_1 b_5 s + b_2 b_4 s\right)\left(m_i^2 - \xi^2\right) + \left(b_2 b_5 s^2 + b_3 b_6 s^2\right)} \quad (26)$$

$$s_i = \frac{b_1 s\left(m_i^2 - \xi^2\right)^2 - \left(b_6 s^2 + b_2 s^2\right)\left(m_i^2 - \xi^2\right)}{b_1 b_4 \left(m_i^2 - \xi^2\right)^2 - \left(b_1 b_5 s + b_2 b_4 s\right)\left(m_i^2 - \xi^2\right) + \left(b_2 b_5 s^2 + b_3 b_6 s^2\right)} \quad (i=1,2,3)\ . \quad (27)$$

The displacement components $\widetilde{\bar{u_1}}$ and $\widetilde{\bar{u_3}}$ are obtained with the aid of (20)-(21) and (24)-(25) as

$\widetilde{\bar{u_1}} = -B_1 i\xi e^{-m_1 x_3} - B_2 i\xi e^{-m_2 x_3} - B_3 i\xi e^{-m_3 x_3} + B_4 m_4 e^{-m_4 x_3}$ (28)

$\widetilde{\bar{u_3}} = -B_1 m_1 e^{-m_1 x_3} - B_2 m_2 e^{-m_2 x_3} - B_3 m_3 e^{-m_3 x_3} - B_4 i\xi e^{-m_4 x_3}$ (29)

Boundary Conditions

The boundary conditions at $x_3 = 0$ are

$\sigma_{33} = -F_1 F(x_1, t), \sigma_{31} = -F_2 F(x_1, t), p = F_3 F(x_1, t), \frac{\partial T}{\partial x_3} = F_4 F(x_1, t)$ (30)

where F_1, F_2 are the magnitudes of the forces , F_3 is the constant pressure applied on the boundary and $F_4$is the constant temperature applied on the boundary. $F(x_1, t)$ is a known of x_1 and t.

Applying Laplace and Fourier transforms defined by (20)and (21) on (30) and with the aid of (10) , we obtain

$\widetilde{\bar{\sigma_{33}}} = -F_1 \tilde{\bar{F}}(\xi, s), \widetilde{\bar{\sigma_{31}}} = -F_2 \tilde{\bar{F}}(\xi, s), \tilde{\bar{p}} = F_3 \tilde{\bar{F}}(\xi, s), \frac{\partial \tilde{\bar{T}}}{\partial x_3} = F_4 \tilde{\bar{F}}(\xi, s)$,at $x_3 = 0$(31)

where

$\widetilde{\bar{\sigma_{33}}} = -R_1 i\xi \widetilde{\bar{u_1}} + R_2 \frac{d\widetilde{\bar{u_3}}}{dx_3} - \alpha \tilde{\bar{p}} - \beta \tilde{\bar{T}}$ (32)

$\widetilde{\bar{\sigma_{31}}} = R_3 \left[\frac{d\widetilde{\bar{u_1}}}{dx_3} - i\xi \widetilde{\bar{u_3}}\right]$ (33)

and $R_1 = \frac{\lambda}{\rho c_1^2}$, $R_2 = \frac{\lambda + 2\mu}{\rho c_1^2}$, $R_3 = \frac{\mu}{\rho c_1^2}$

Case 1: For normal force $F_2 = F_3 = F_4 = 0$

Case 2: For tangential force $F_1 = F_3 = F_4 = 0$

Case 3: For pressure source $F_1 = F_2 = F_4 = 0$
Case 4: For thermal source $F_1 = F_2 = F_3 = 0$
Substituting the values of $\widetilde{\widetilde{u_1}}$, $\widetilde{\widetilde{u_3}}$,$\tilde{\tilde{p}}$ and $\tilde{\tilde{T}}$ from(28),(29) and (24) in the boundary condition (31) and with help of (32) and (33), after some simplifications, we obtain

$$\widetilde{\widetilde{\sigma_{33}}} = \frac{1}{\Delta}[d_1\Delta_1 e^{-m_1x_3} + d_2\Delta_2 e^{-m_2x_3} + d_3\Delta_3 e^{-m_3x_3} + d_4\Delta_4 e^{-m_4x_3}] \quad (34)$$

$$\widetilde{\widetilde{\sigma_{31}}} = \frac{1}{\Delta}[d_5\Delta_1 e^{-m_1x_3} + d_6\Delta_2 e^{-m_2x_3} + d_7\Delta_3 e^{-m_3x_3} + d_8\Delta_4 e^{-m_4x_3}] \quad (35)$$

$$\tilde{\tilde{p}} = \frac{1}{\Delta}[r_1\Delta_1 e^{-m_1x_3} + r_2\Delta_2 e^{-m_2x_3} + r_3\Delta_3 e^{-m_3x_3}] \quad (36)$$

$$\tilde{\tilde{T}} = \frac{1}{\Delta}[s_1\Delta_1 e^{-m_1x_3} + s_2\Delta_2 e^{-m_2x_3} + s_3\Delta_3 e^{-m_3x_3}] \quad (37)$$

where

$\Delta = d_1d_8(-m_3r_2s_3 + m_2r_3s_2) - d_2d_8(-m_3r_1s_3 + m_1r_3s_1) + d_3d_8(-m_2r_1s_2 + m_1r_2s_1) - d_4d_5(-m_3r_2s_3 + m_2r_3s_2) - d_4d_6(-m_1r_3s_1 + m_3r_1s_3) - d_4d_7(-m_2r_1s_2 + m_1r_2s_1)$,

$d_i = -R_1\xi^2 + R_2m_i^2 - \alpha r_i - s_i$ where (i=1,2,3) , $d_4 = i\xi m_4(-R_1 + R_2)$

$d_j = 2i\xi m_jR_3$ where (j=5,6,7) , $d_8 = -R_3(m_4^2 + \xi^2)$,

and $\Delta_1, \Delta_2, \Delta_3, \Delta_4$ are obtained by replacing $[-F_1, -F_2, F_3, F_4]^T$ in Δ.

Applications:

Case1.Concentrated Source:

The values for displacement, stress, pore pressure and temperature change presented in equations (34)-(37) will used to yield the response over the half space subjected to a concentrated source as

$$F(x_1, t) = \delta(x_1)\delta(t), \quad (38)$$

where $\delta(\ )$ is the Dirac-delta function.

Applying the Laplace and Fourier tranceform defined by (20) and (21) on (38), yield $\tilde{\tilde{F}}(\xi, s) = 1$ (39)

The component of displacement, stress, pore pressure and temperature change are obtained by using (39) in (34)-(37).

Case2.Influence function:

Here $F(x_1, t) = \Psi_1(x_1)\delta(t)$ (40) where $\Psi_1(x_1)$ is a known function and take two type of values

1.Uniformly distributed source

$$\Psi_1(x_1) = \begin{Bmatrix} 1, |x_1| \le a \\ 0, |x_1| > a \end{Bmatrix}, \quad (41)$$

where 2a is non-dimensional width of the strip.

Applying the Laplace and Fourier transform defined by (20) and (21) on (40) and (41), we obtain

$$\tilde{\tilde{F}}(\xi, s) = [(2sin\xi a)/\xi] \quad (42)$$

2. Linearly distributed source

$$\Psi_1(x_1) = \begin{Bmatrix} 1 - \frac{|x_1|}{a}, |x_1| \le a \\ 0, \quad |x_1| > a \end{Bmatrix}, \quad (43)$$

where 2a is non-dimensional width of the strip.

Applying the Laplace and Fourier trance defined by (20) and (21) on (40) and (43), we obtain

$$\tilde{\tilde{F}}(\xi, s) = \frac{2[1 - cos(\xi a)]}{\xi^2 a} \quad (44)$$

The expression for stresses, pore pressure and temperature can be obtained for concentrated, uniformly and linearly distributed source by replacing $\tilde{\tilde{F}}(\xi, s)$ from (39),(42) and (44) in (34)-(37).

SPECIAL CASE

In the absence of porosity effect, the boundary conditions reduce to

$$\widetilde{\sigma_{33}} = -F_1\tilde{\tilde{F}}(\xi, s), \widetilde{\sigma_{31}} = -F_2\tilde{\tilde{F}}(\xi, s), \frac{\partial\tilde{\tilde{T}}}{\partial x_3} = F_4\tilde{\tilde{F}}(\xi, s) \quad (45)$$

and we obtain the corresponding expressions for stress components in thermoelastic half space as

$$\widetilde{\sigma_{zz}} = \frac{1}{\Delta_{10}}[d_9\Delta_5 e^{-m_5x_3} + d_{10}\Delta_6 e^{-m_6x_3} + d_4\Delta_7 e^{-m_4x_3}] \quad (46)$$

$$\widetilde{\sigma_{zr}} = \frac{1}{\Delta_{10}}[d_{11}\Delta_5 e^{-m_5x_3} + d_{12}\Delta_6 e^{-m_6x_3} + d_8\Delta_7 e^{-m_4x_3}] \quad (47)$$

$$\tilde{\tilde{T}} = \frac{1}{\Delta_{10}}[r_5\Delta_5 e^{-m_5x_3} + r_6\Delta_6 e^{-m_6x_3}] \quad (48)$$

where

$d_9 = -R_1\xi^2 + R_2m_5^2 - r_5$, $d_{10} = -R_1\xi^2 + R_2m_6^2 - r_6$, $d_{11} = 2i\xi m_5R_3$, $d_{12} = 2i\xi m_6R_3$.

$\Delta_{10} = d_9d_8m_6r_6 - d_{10}d_8m_5r_5 - d_4d_{11}m_6r_6 + d_4d_{12}m_5r_5$,

and $\Delta_5, \Delta_6, \Delta_7$ are obtained by replacing $[-F_1, -F_2, F_4]^T$ in Δ_{10}.

Taking $F_2 = F_4 = 0$, $F_1 = F_4 = 0$, $F_1 = F_2 = 0$ in equations (46)-(48) respectively , we obtain the stress components and temperature change for normal force, tangential forces and thermal source respectively.

Inversion of the transform

The transformed stresses, pore pressure and temperature are functions of the parameters of the Laplace and Fourier transforms s and ξ respectively and hence are of the form $\tilde{\tilde{f}}(\xi, z, s)$.To obtain the solution of the problem in the physical domain, we invert the Laplace and Hankel transforms by using the method described by Kumar et.al. [23].

Numerical results and discussion

With the view of illustrating the theoretical results and for numerical discussion we take a model for which the value of the various physical parameters are taken from Jabbari and dehbani [22]:

$E = 6 \times 10^5$, $\nu = 0.3$, $T_0 = 293$, $K_s = 2 \times 10^{10}$, $K_w = 5 \times 10^9$, $K = 0.5$,

$\alpha_s = 1.5 \times 10^{-5}$, $\alpha_W = 2 \times 10^{-4}$, $c_s = 0.8$, $c_w = 4.2$, $\rho_s = 2.6 \times 10^6$, $\rho_w = 1 \times 10^6$

$\alpha = 1, F_1 = F_2 = F_3 = F_4 = 1.$

The values of normal stress σ_{33} , tangential stress σ_{31} , pore pressure p and temperature change T for incompressible fluid saturated thermoporoelastic medium (FSPM) and empty porous thermoelastic medium (EPM) are shown due to concentrated source (CS), uniformly distributed source (UDS), and linearly distributed source (LDS) .The computation are carried out for two values of dimensionless time t=0.5 and t=0.75 at $x_3 = 1$ in the range $0 \le x_1 \le 10$, a=1.

The solid lines either with or without central symbols represents the variations for t=0.5, whereas the dashed lines with or without central symbols represents the variations for t=0.75.Curves without central symbols correspond to the case of FSPM whereas those with central symbols corresponds to the case of EPM.

Fig.2 shows the variation of normal stress component σ_{33} w.r.t distance x_1 for both FSPM and EPM due to concentrated normal force. The value of σ_{33} increases in oscillatory manner for FSPM as x_1

increases and in case of EPM, the value of σ_{33} decrease in the range $0 \leq x_1 \leq 2.3$ and then oscillates as x_1 increases for both values of time.

Fig.3 shows the variation of normal stress component σ_{33} w.r.t distance x_1 for both FSPM and EPM due to concentrated tangential force. The value of σ_{33} decrease in the range $0 \leq x_1 \leq 2.5$ and then oscillate for FSPM as x_1 increases for both values of time whereas in case of EPM, the value of σ_{33} oscillates oppositely for different values of time as x_1 increases.

Fig.4 shows the variation of normal stress component σ_{33} w.r.t distance x_1 for FSPM due to concentrated pressure source. The value of σ_{33} decreases in the range $0 \leq x_1 \leq 2.1$ and then oscillate for different values of time.

Fig.5 shows the variation of normal stress component σ_{33} w.r.t distance x_1 for FSPM and EPM due to concentrated thermal source. The value of σ_{33} oscillates oppositely for different values of time as x_1 increases whereas in case of EPM, the value of σ_{33} first increases in the range $0 \leq x_1 \leq 2$ and then oscillate for both values of time as x_1 increases.

Fig.6 shows the variation of pore pressure p w.r.t distance x_1 for FSPM due to concentrated normal force. The value of p is more for the time t=0.5 as compared to time t=0.75 in the range $0 \leq x_1 \leq 4.5$ and then reverse trend is noticed as x_1 increases.

Fig.7 shows the variation of pore pressure p w.r.t distance x_1 for FSPM due to concentrated tangential force. The value of p first increases and then oscillates for both values of time as x_1 increases.

Fig.8 shows the variation of pore pressure p w.r.t distance x_1 for FSPM due to concentrated pressure source. The value of p is more for the time t=0.75 as compared to time t=0.5 in the range $0 \leq x_1 \leq 5$ and then reverse trend is noticed as x_1 increases.

Fig.9 shows the variation of pore pressure p w.r.t distance x_1 for FSPM due to concentrated thermal source. For the time t=0.5 the value of p is more in the range $0 \leq x_1 \leq 7.5$ whereas for the time t=0.75 the value of p is more in the range $7.5 \leq x_1 \leq 10$.

Fig.10 shows the variation of temperature T w.r.t distance x_1 for FSPM and EPM due to concentrated normal force. The value of T first decreases and then oscillates for FSPM as x_1 increases for both value of time whereas for EPM the value of T is more for the time t=0.5 as compared to time t=0.75 in the range $0 \leq x_1 \leq 4.2$ and then reverse trend is noticed as x_1 increases.

Fig.11 shows the variation of temperature T w.r.t distance x_1 for FSPM and EPM due to concentrated tangential force. The value of T increases in the range $0 \leq x_1 \leq 2.3$, decreases in the range $2.3 \leq x_1 \leq 6$ and then oscillates for FSPM as x_1 increases for different values of time. For EPM the value of T first decreases in the range $0 \leq x_1 \leq 2$ and then oscillates as x_1 increases for both value of time.

Fig.12 shows the variation of temperature T w.r.t distance x_1 for FSPM due to concentrated pressure source. The value of T is more for the time t=0.75 as compared to time t=0.5 in the range $0 \leq x_1 \leq 2.5$ and then reverse trend is noticed as x_1 increases.

Fig.13 shows the variation of temperature T w.r.t distance x_1 for FSPM and EPM due to concentrated thermal source. The value of T decreases exponentially for FSPM as x_1 increases for both value time whereas for EPM the value of T increases in the range $0 \leq x_1 \leq 3$ and then oscillates oppositely for both value of time as x_1 increases.

Fig.14 shows the variation of normal stress component σ_{33} w.r.t distance x_1 for FSPM and EPM due to normal force over uniformly distributed source. The value of σ_{33} increases in oscillatory manner for FSPM as x_1 increases whereas for EPM it decreases sharply in the range $0 \leq x_1 \leq 23$ and then oscillates for both values of time as x_1 increases.

Fig.15 shows the variation of normal stress component σ_{33} w.r.t distance x_1 for FSPM and EPM due to tangential force over uniformly distributed source. The value of σ_{33} first decreases in the range $0 \leq x_1 \leq 2.5$ and then oscillates for FSPM as x_1 increases for both values of time whereas for EPM it oscillates oppositely as x_1 increases for the time t=0.5 and t=0.75.

Fig.16 shows the variation of normal stress component σ_{33} w.r.t distance x_1 for FSPM due to pressure source over uniformly distributed source. The value of σ_{33} is more for the time t=0.5 as compared to time t=0.75 in the range $0 \leq x_1 \leq 7.5$ and then reverse trend is noticed as x_1 increases.

Fig.17 shows the variation of normal stress component σ_{33} w.r.t distance x_1 for FSPM and EPM due to thermal source over uniformly distributed source. The value of σ_{33} oscillates oppositely for different values of time as x_1 increases whereas in case of EPM, the value of σ_{33} first increases in the range $0 \leq x_1 \leq 2$ and then oscillate for both values of time as x_1 increases.

Fig.18 shows the variation of pore pressure p w.r.t distance x_1 for FSPM due to normal force over uniformly distributed source. The value of p shows a sharp decrease for time t=0.5 whereas for t=0.75 the value of p first increases then decreases for FSPM as x_1 increases.

Fig.19 shows the variation of pore pressure p w.r.t distance x_1 for FSPM due to tangential force over uniformly distributed source. The value of p increases in the range $0 \leq x_1 \leq 3$, decreases in the range $3 \leq x_1 \leq 5.5$ and then oscillates for FSPM as x_1 increases for the time t=0.5 and t=0.75.

Fig.20 shows the variation of pore pressure p w.r.t distance x_1 for FSPM due to pressure source over uniformly distributed source. Near the application of the source the value of p is more for the time t=0.75 as compared to time t=0.5 in the range $0 \leq x_1 \leq 5$ and then reverse trend is noticed away from the source.

Fig.21 shows the variation of pore pressure p w.r.t distance x_1 for FSPM due to thermal source over uniformly distributed source. The value of p converges near the boundary surface for the time t=0.5 whereas for time t=0.75 the value of p increases in the range $0 \leq x_1 \leq 4.5$ and then oscillates as x_1 increases.

Fig.22. shows the variation of temperature T w.r.t distance x_1 for FSPM and EPM due to normal force over uniformly distributed source. The value of T first increases in the range $0 \leq x_1 \leq 2$ and then

start decreasing for FSPM whereas for EPM the value of T increases exponentially as x_1 increases for different values of time.

Fig.23 shows the variation of temperature T w.r.t distance x_1 for FSPM and EPM due to tangential force over uniformly distributed source. The value of T increases in the range $0 \leq x_1 \leq 2.3$, decreases in the range $2.3 \leq x_1 \leq 6$ and then oscillates for FSPM as x_1 increases for different values of time. For EPM the value of T first decreases in the range $0 \leq x_1 \leq 2$ and then oscillates as x_1 increases for both value of time.

Fig.24 shows the variation of temperature T w.r.t distance x_1 for FSPM due to pressure source over uniformly distributed source. The value of T is more for the time t=0.75 as compared to time t=0.5 in the range $0 \leq x_1 \leq 2.5$ and then reverse trend is noticed as x_1 increases.

Fig.25 shows the variation of temperature T w.r.t distance x_1 for FSPM and EPM due to thermal source over uniformly distributed source. The value of T decreases gradually for FSPM as x_1 increases whereas for EPM value of T first increases in the range $0 \leq x_1 \leq 2.5$ and then becomes linear as x_1 increases for different values of time.

Fig.26 shows the variation of normal stress component σ_{33}w.r.t distance x_1 for FSPM and EPM due to normal force over linearly distributed source. The value of σ_{33} is more for the time t=0.75 as compared to time t=0.5 in the range $0 \leq x_1 \leq 4.8$ and then reverse trend is noticed as x_1 increases. For EPM the value of σ_{33} decreases sharply in the range $0 \leq x_1 \leq 23$ and then oscillates for both values of time as x_1 increases.

Fig.27 shows the variation of normal stress component σ_{33}w.r.t distance x_1 for FSPM and EPM due to tangential force over linearly distributed source. The value of σ_{33} for FSPM oscillates about the origin as x_1 increases for both values of time whereas in case of EPM, the value of σ_{33} oscillates oppositely for different values of time as x_1 increases.

Fig.28 shows the variation of normal stress component σ_{33} w.r.t distance x_1 for FSPM due to pressure source over linearly distributed source. The value of σ_{33} decreases in the range $0 \leq x_1 \leq 6$, increases in the range $6 \leq x_1 \leq 8$ and then oscillates for FSPM as x_1 increases for different values of time.

Fig.29 shows the variation of normal stress component σ_{33} w.r.t distance x_1 for FSPM and EPM due to thermal source over linearly distributed source. The value of σ_{33} for FSPM oscillates oppositely about the origin as x_1 increases for both values of time whereas the value of σ_{33} first increases in the range $0 \leq x_1 \leq 2$ and then oscillates for EPM as x_1 increases for both values of time.

Fig.30 shows the variation of pore pressure p w.r.t distance x_1 for FSPM due to normal force over linearly distributed source. The value of p shows a sharp decrease for time t=0.5 whereas for t=0.75 the value of p first increases then decreases for FSPM as x_1 increases.

Fig.31 shows the variation of pore pressure p w.r.t distance x_1 for FSPM due to tangential force over linearly distributed source. The value of p is more for the time t=0.5 as compared to time t=0.75 in the range $0 \leq x_1 \leq 4$ and then reverse trend is noticed as x_1 increases.

Fig.32 shows the variation of pore pressure p w.r.t distance x_1 for FSPM due to pressure source over linearly distributed source. The value of p first decreases and then starts increasing as x_1 increases for both values of time.

Fig.33 shows the variation of pore pressure p w.r.t distance x_1 for FSPM due to thermal source over linearly distributed source. For the time t=0.5 the value of p is more in the range $0 \leq x_1 \leq 7.5$ whereas for the time t=0.75 the value of p is more in the range $7.5 \leq x_1 \leq 10$.

Fig.34 shows the variation of temperature T w.r.t distance x_1 for FSPM and EPM due to normal force over linearly distributed source. The value of T first decreases and then oscillates for FSPM as x_1 increases for both value of time whereas for EPM the value of T increases exponentially for t=0.5 and t=0.75 as x_1 increases.

Fig.35 shows the variation of temperature T w.r.t distance x_1 for FSPM and EPM due to tangential force over linearly distributed source. The value of T increases in converges near the boundary surface for FSPM as x_1 increases for different values of time whereas for EPM the value of T first decreases in the range $0 \leq x_1 \leq 2$ and then oscillates as x_1 increases for both value of time.

Fig.36 shows the variation of temperature T w.r.t distance x_1 for FSPM due to pressure source over linearly distributed source. . The value of T is more for the time t=0.75 as compared to time t=0.5 in the range $0 \leq x_1 \leq 2.5$ and then reverse trend is noticed as x_1 increases.

Fig.37 shows the variation of temperature T w.r.t distance x_1 for FSPM and EPM due to thermal source over linearly distributed source. The value of T decreases exponentially for FSPM as x_1 increases for both value time whereas for EPM the value of T increases in the range $0 \leq x_1 \leq 3$ and then oscillates oppositely for both value of time as x_1 increases.

Conclusion:

The components of displacement, stress, pore pressure and temperature change are obtained due to the various sources by using the Laplace and Fourier transforms. The values of the components of displacement, stress, pore pressure and temperature are close to each other due to CS, UDS and LDS. Near the application of the source, the porosity effect decreases the values of σ_{33} for normal force, pressure source and thermal source where as it decrease the values of p for normal force and tangential force but increase the values for thermal source.

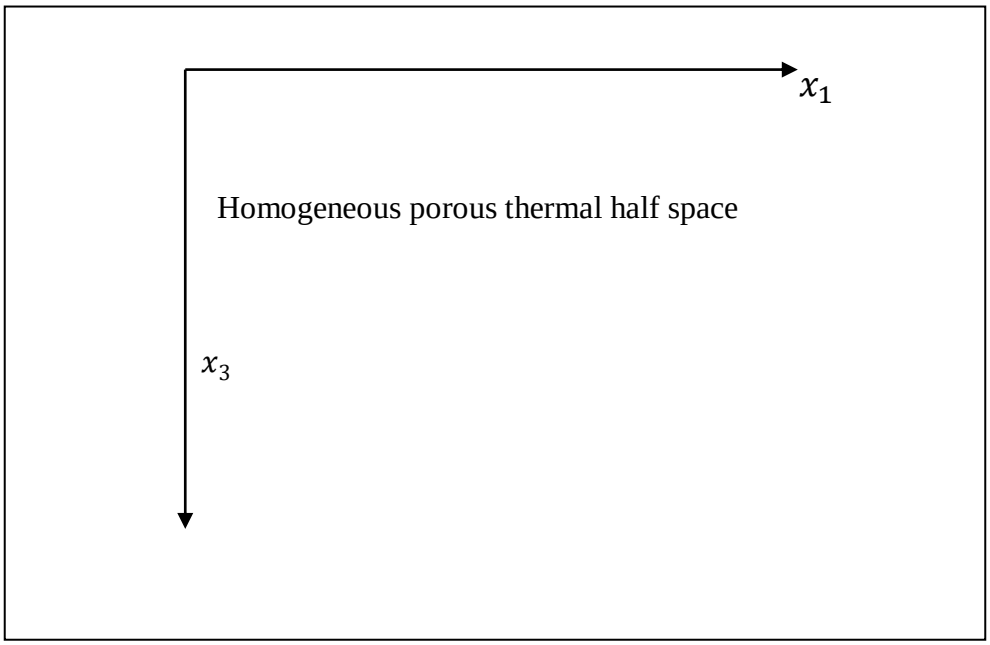

Fig. 1. Geometry of the problem

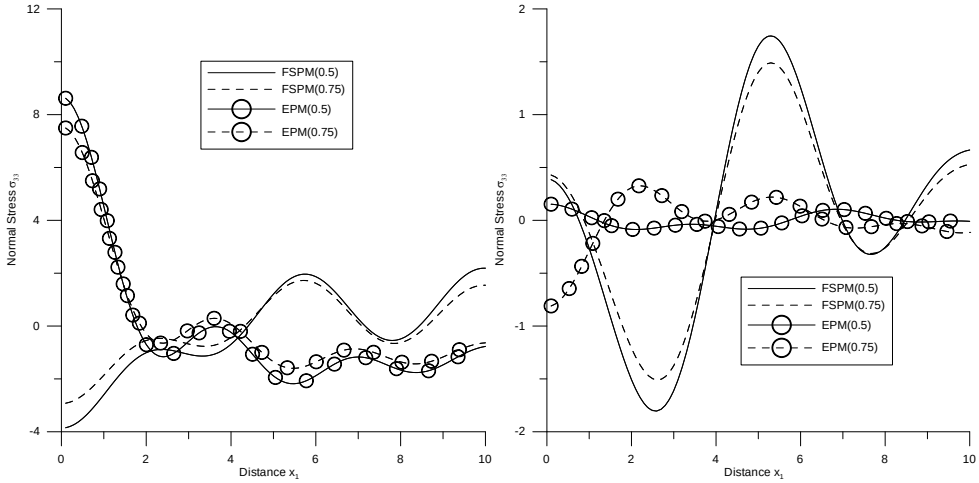

Fig. 2 Variation of normal stress σ_{33} with distance x_1 due to concentrated normal force. Fig. 3 Variation of normal stress σ_{33} with distance x_1 due to concentrated tangential force

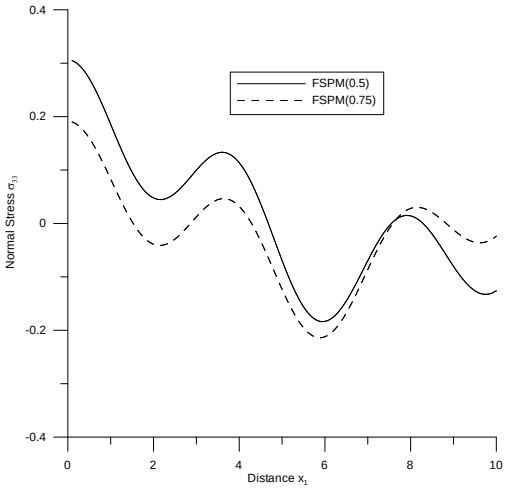

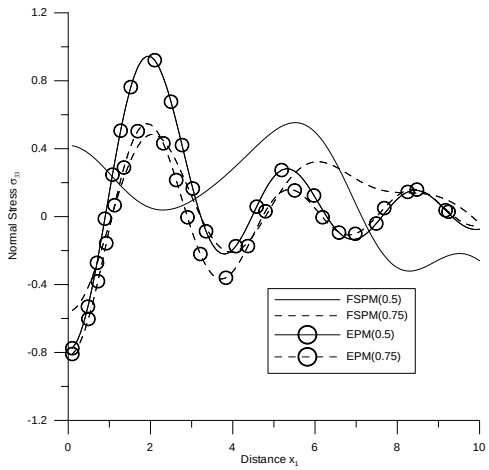

Fig.4 Variation of normal stress σ_{33} with distance x_1 due to concentrated pressure source. Fig.5 Variation of normal stress σ_{33} with distance x_1 due to thermal source.

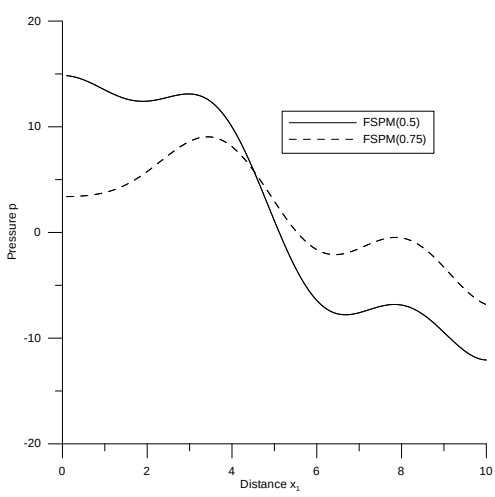

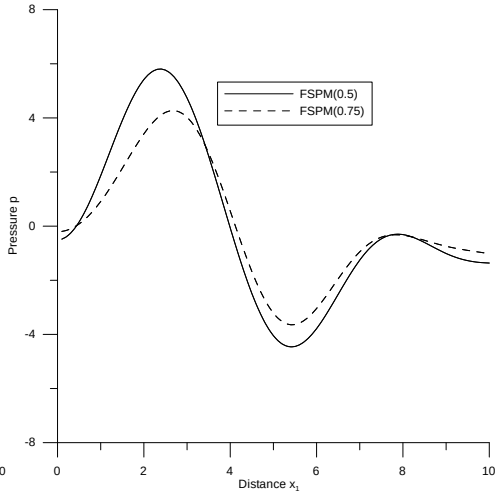

Fig 6.Variation of pore pressure p with distance x_1 due to concentrated normal force Fig 7.Variation of pore pressure p with distance x_1 due to concentrated tangential force

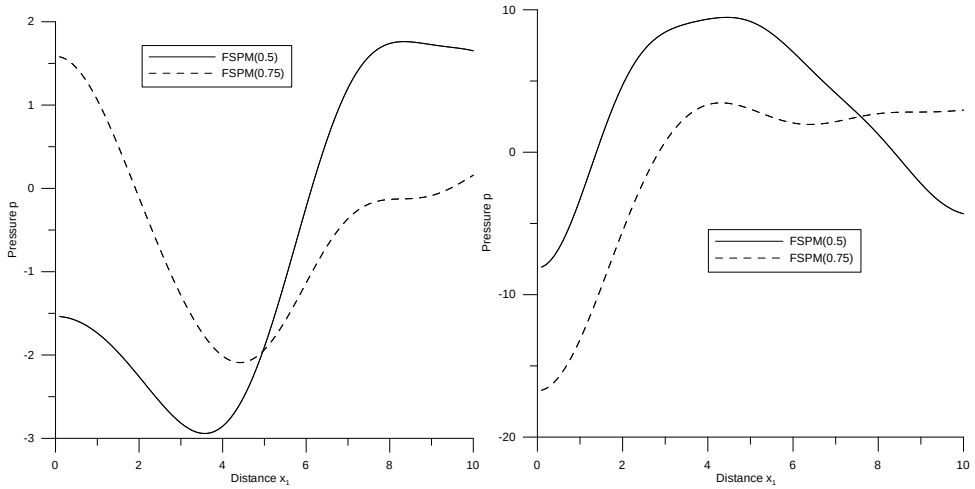

Fig 8.Variation of pore pressure p with distance x_1 due to concentrated pressure source Fig 9.Variation of pore pressure p with distance x_1 due to thermal source

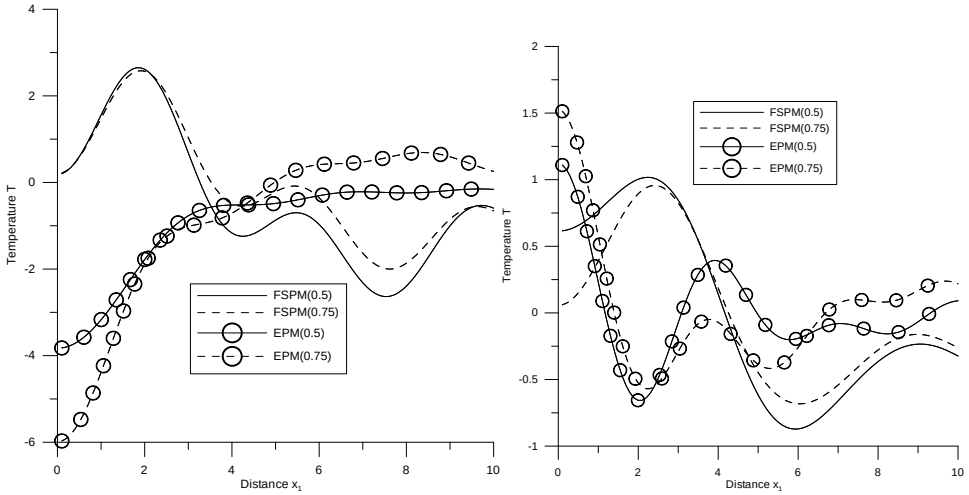

Fig. 10 Variation of temperature with distance x_1 due to concentrated normal force Fig. 11 Variation of temperature with distance x_1 due to concentrated tangential force

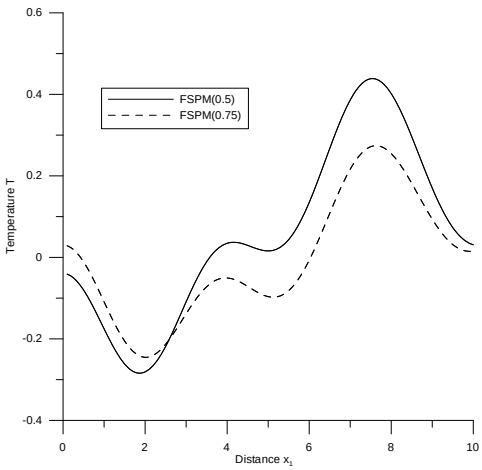

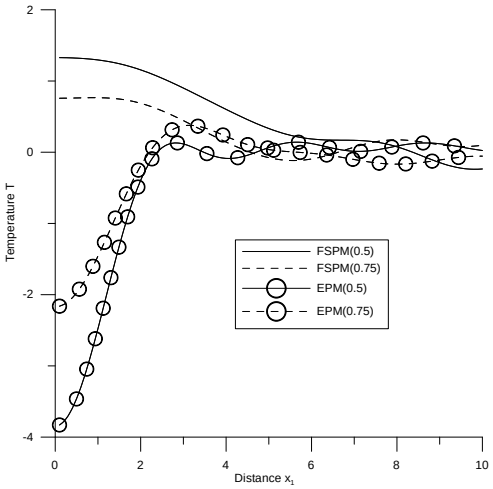

Fig. 12 Variation of temperature with distance x_1 due to concentrated pressure source Fig. 13 Variation of temperature with distance x_1 due to thermal source

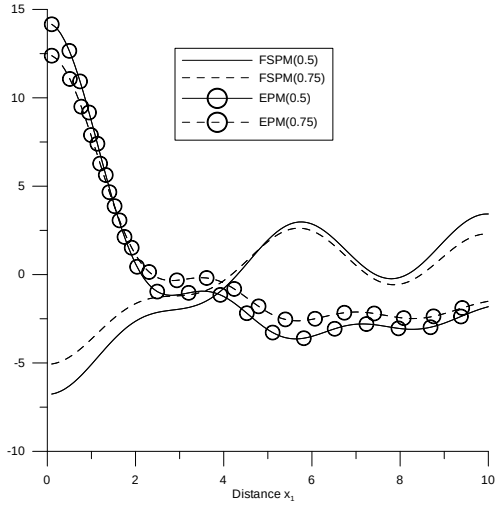

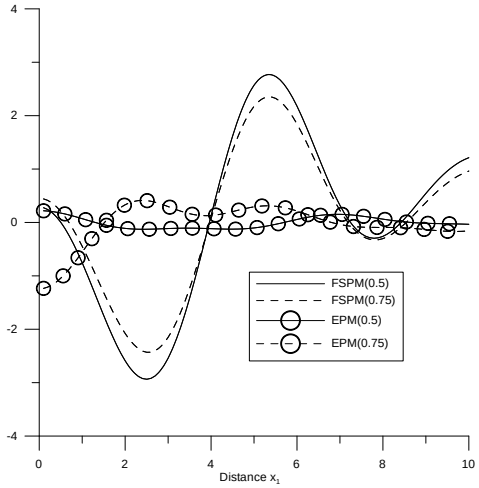

Fig 14 Variation of normal stress wσ_{33}ith distance $x_1$due to concentrated normal force. Fig. 15 Variation of normal stress σ_{33} with distance x_1 due to concentrated tangential force.

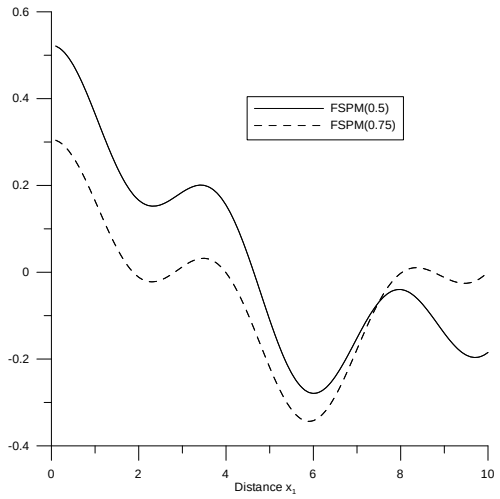

Fig. 16 Variation of normal stress σ_{33} with distance x_1 due to concentrated pressure source

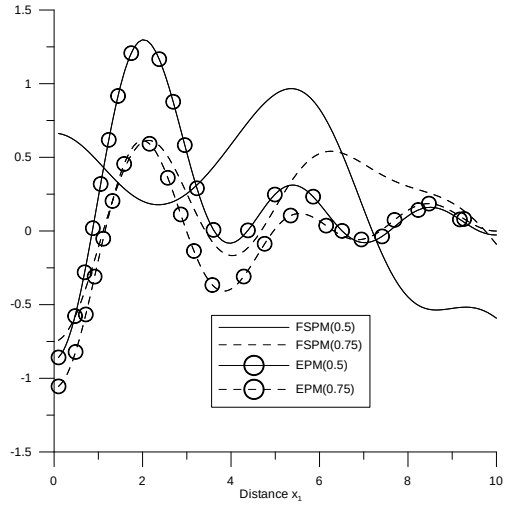

Fig. 17 Variation of normal stress σ_{33} with distance x_1 due to thermal source

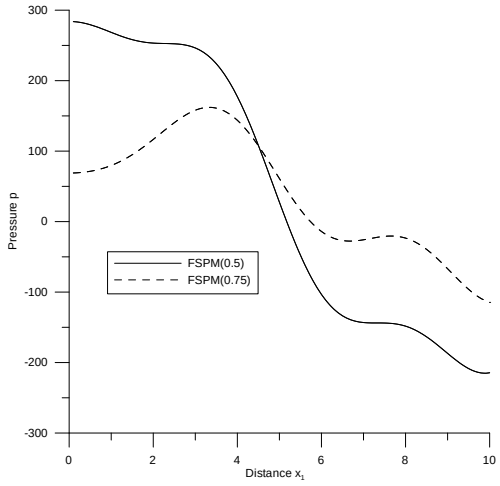

Fig 18.Variation of pore pressure p with distance x_1 due to concentrated normal force

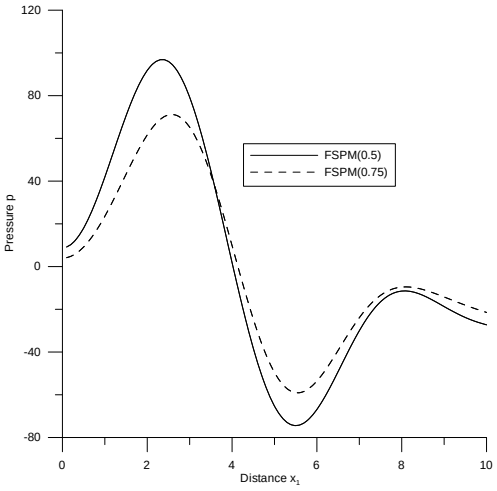

Fig 19.Variation of pore pressure p with distance x_1 due to concentrated tangential force

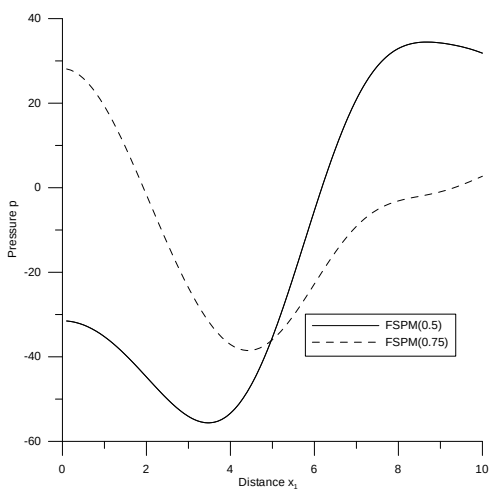

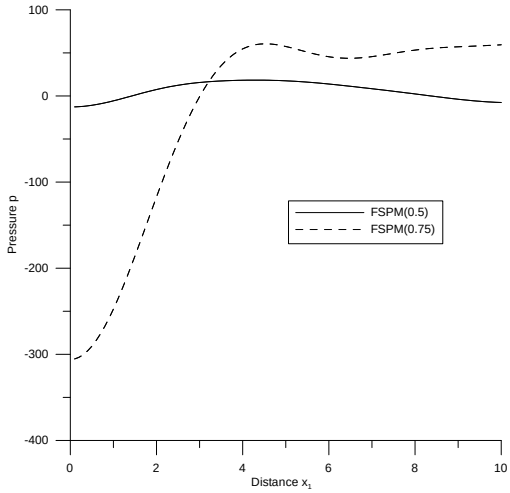

Fig 20.Variation of pore pressure p with distance x_1 due to concentrated pressure source.

Fig 21.Variation of pore pressure p with distance x_1 due to thermal source

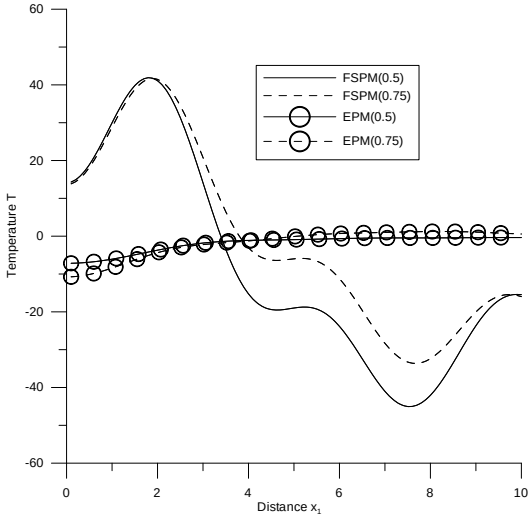

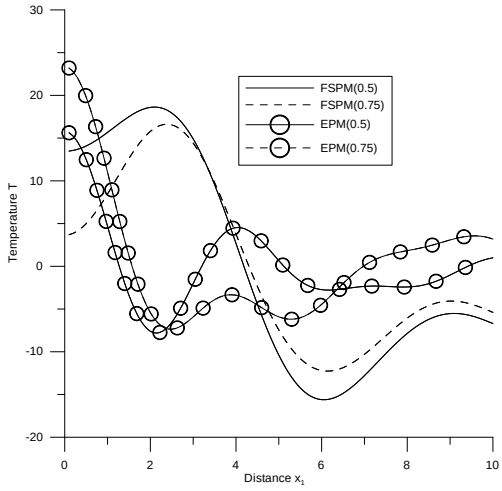

Fig. 22 Variation of temperature with distance x_1 due to concentrated normal force **Fig. 23 Variation of temperature with distance x_1 due to concentrated tangential force**

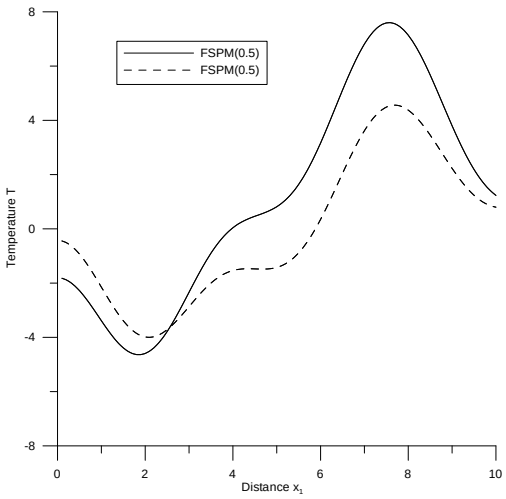

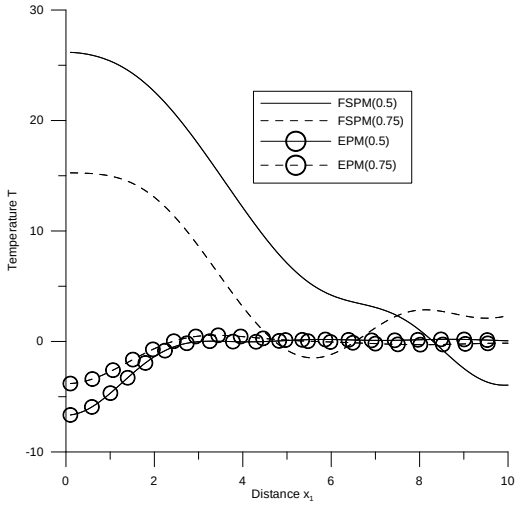

Fig. 24 Variation of temperature with distance x_1 due to concentrated pressure source
Fig. 25 Variation of temperature with distance x_1 due to thermal source

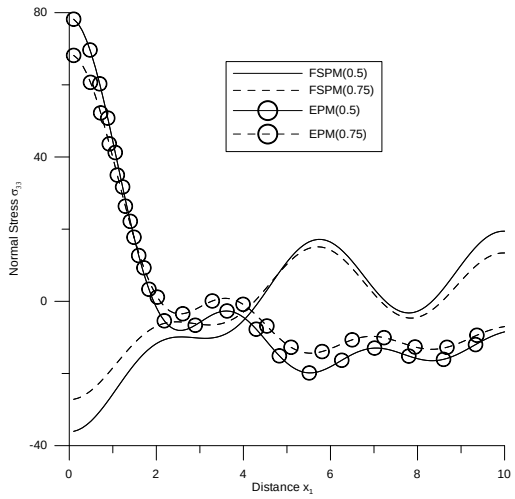

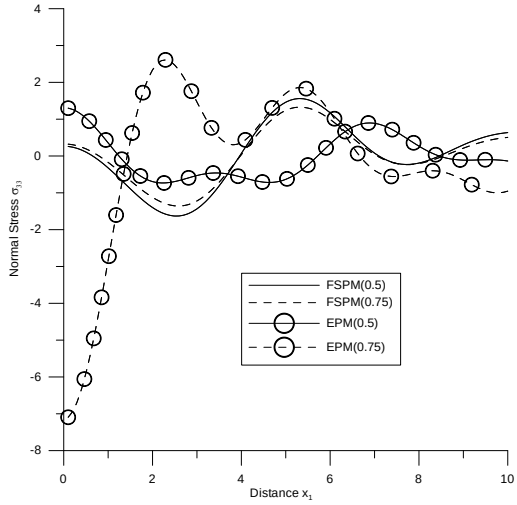

Fig. 26 Variation of normal stress σ_{33} with distance x_1 due to concentrated normal force

Fig. 27 Variation of normal stress σ_{33} with distance x_1 due to concentrated tangential force.

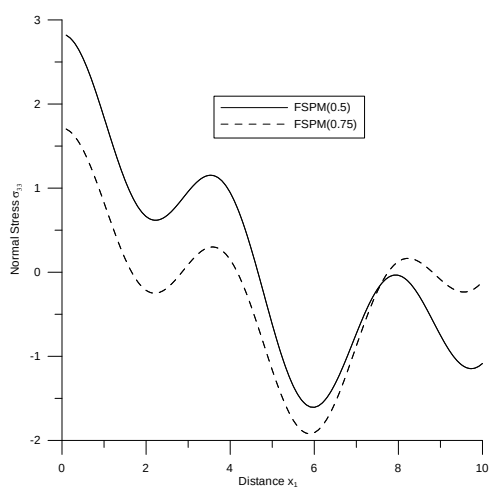

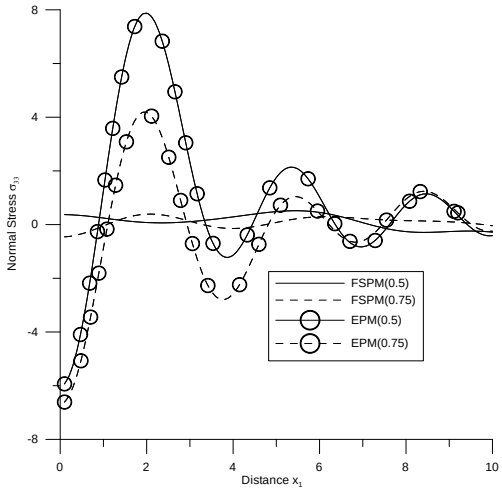

Fig. 28 Variation of normal stress $\sigma_{33}$with distance x_1 due to concentrated pressure source.

Fig. 29 Variation of normal stress wiσ_{33}th distance x_1 due to thermal source.

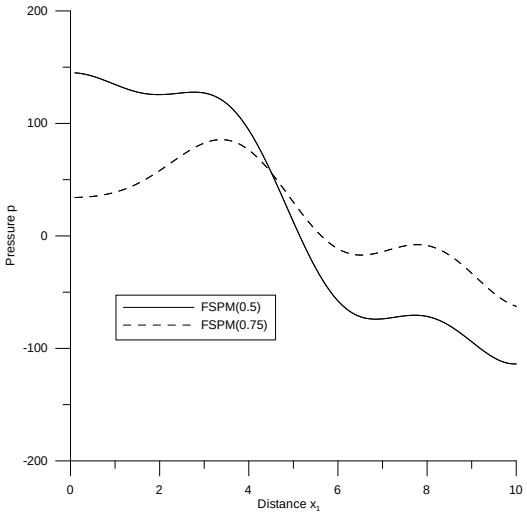

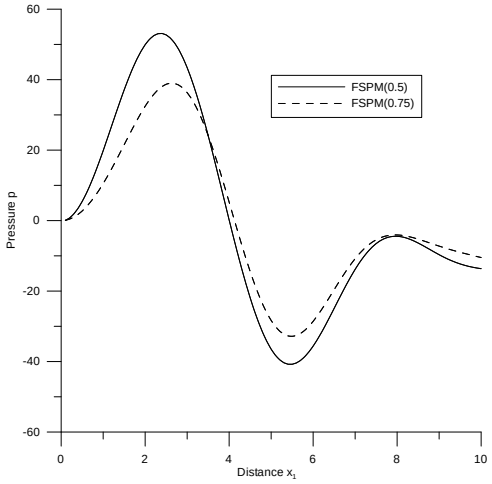

Fig 30 Variation of pore pressure p with distance $x_1$due to concentrated normal force

Fig 31.Variation of pore pressure p with distance xx_1 due to concentrated tangential force

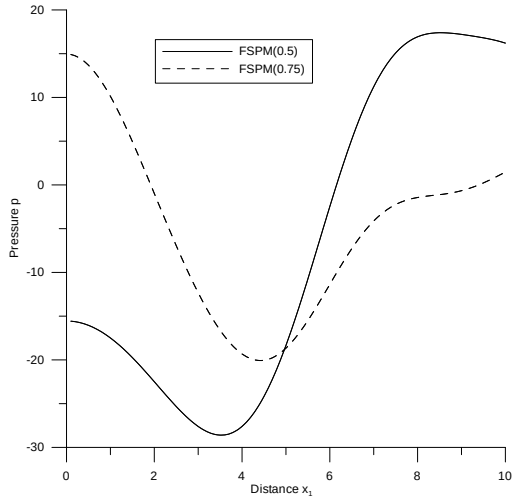

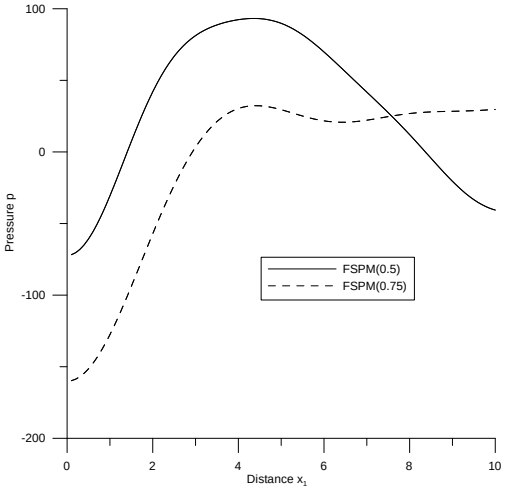

Fig 32.Variation of pore pressure p with distance x_1 due to concentrated pressure source

Fig 33.Variation of pore pressure p with distance x_1 due to thermal source

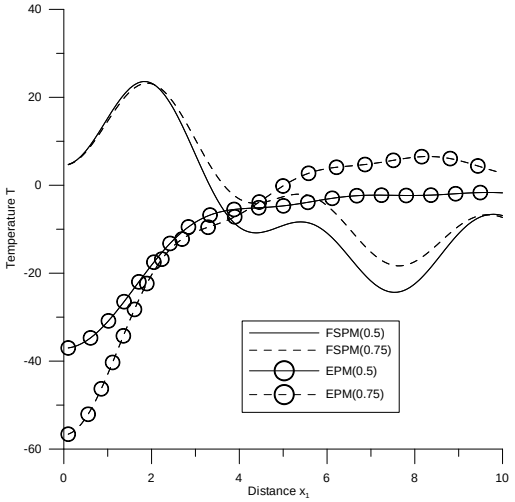

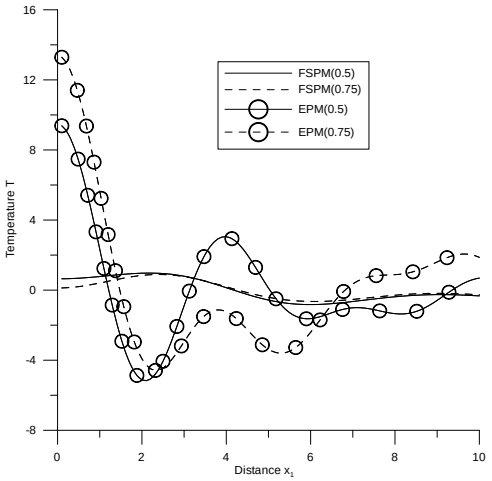

Fig. 34 variation of temperature with distance x_1 due to concentrated normal force

Fig. 35 variation of temperature with distance x_1 due to concentrated tangential force

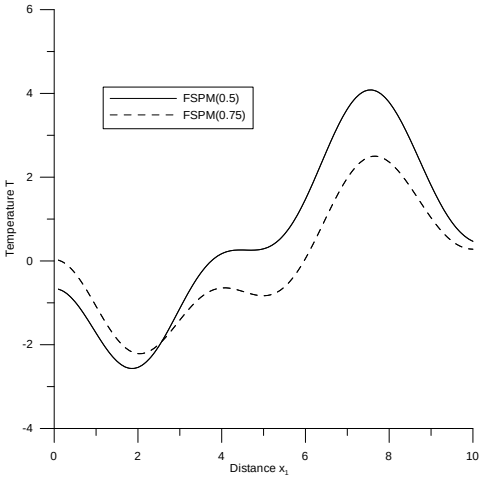

Fig. 36 variation of temperature with distance x_1 due to concentrated pressure source

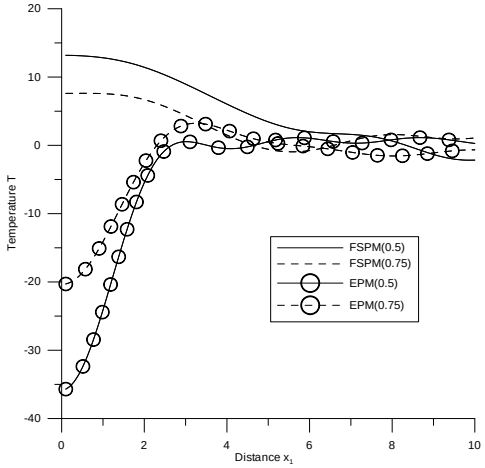

Fig. 37 variation of temperature with distance x_1 due thermal source

References:

1. Terzaghi, K.V., Die Berechnug der Durchlassigkeit des Tones aus dem Verlauf der hydromechanischen Spannungserscheinungen, Sitzungsber Akad. Wiss. (Wien),Math.-Naturwiss.K.,Abt.IIa, 132, 125-138, 1923.
2. Terzaghi, K.V.,Erdbaumechanik auf Bodenphysikalischer Grundlage, p. 399 Leipzig-wien :Franz Deuticke (1925).
3. Biot, M.A. ,General theory of three dimensional consolidation, J. Appl. Phys., 12(2), 155-161, 1941.
4. Biot, M.A., Theory of propagation of elastic waves in fluid saturated porous solid I-low frequency range, Journal of the Acoustical Society of America, 28, 168-178,1956a.
5. Biot , M.A.,Theory of propagation of elastic waves in fluid saturated porous solid II-Higher frequency range, Journal of the Acoustical Society of America, 28, 179-191,1956b.
6. Biot , M.A., Mechanics of deformation and acoustic propagation in porous media, J. Appl. Phys., 33(4), 1482-1498,1962.
7. Kumar, R. and Hundal , B.S., The wave propagation in a fluid saturated incompressible porous medium,Indian J.pure and applied math., 4, 51-65,2003.
8. Bai and Li .T. , Solution for cylindrical cavety in saturated thermoporoelastic medium,Acta Mech. Solida Sinica, 22, (1), 85-92, 2009.
9. Bai , B., Response of saturated porous media subjected to local thermal loading on the surface of semi-space, Acta mechanica sinica, 22, 54-61,2006.
10. Bai , B., Thermal response of saturated porous spherical body containing a cavity under several boundary conditions, Journal of thermal stresses, 36 (11), 1217-1232,2013.
11. Bai , B., Fluctuation responses of porous media subjected to cyclic thermal loading, Computers and geotechnics, 33, 396-403,2006.
12. Kaushal , B. , Kumar, R. and Miglani, A. , Responce of frequency domain in generalized thermoelasticity with two temperature, Journal of Eng. Physics and Thermophysics, 83 (5), 1080-1088,2010.

13. Jabbari, M. and Dehbani , H., An exact solution for classic coupled thermoelasticity in axisymmetric cylinder, Journal of Solid Mechanics, 2 (2), 129-143,2010.
14. Jabbari, M. and Dehbani , H., An exact solution for quasi-static poro- thermoelasticity in spherical coordinate, Iranian Journal of Mechanical Engineering , 12(1), 86-108,2011.
15. Apostolakis G. and Dargus , G.F. (2013), " Mixed variation principal for dynamic response of thermoelastic and poroelastic continua", Int. J. of Solid and Structure , vol.50, No. 5, pp. 642-650.
16. Hou, P.F. , Zhao, M. and Jiann-Wen , J.U. (2013), " The three dimensional green's function for transversely isotropic thermoporoelastic biomaterial", J.Appl. Geophysics , vol. 95, pp. 36-46.
17. Jabbari M., Hashemitaheri M., Mojahedin A., Eslami M.R., 2014, "Thermal buckling analysis of functionally graded thin circular plate made of saturated porous materials", Journal of thermal stresses, vol. 37, pp. 202-220.
18. Liu, M., and Chain , C.(2015), "A micromechanical analysis of the fracture properties of saturated porous media", Int. J. of Solid and Structure, vol. 63, pp. 32-38.
19. He, S.M., Liu, W. and Wang , J.(2015), "Dynamic simulation of landslide based on thermoporoelastic approach", Computers and Geosciences, vol. 75, pp. 24-32.
20. Nguyen, H.T., Wong , H., Fabbri , A., Georgin, J.F. and Prudhomme , E.(2015), "Analytical study of freezing behaviour of a cavity in thermoporoelastic medium", Computers and Geotechnics , vol. 67, pp. 33-45.
21. Wu, D., Yu , L., Wang , Y., Zhao, B. and Gao , Y. (2015), "A refined theory of axisymmetric thermoporoelastic circular cylinder",European J. Mech. A/Solid ,In Press , Accepted Manuscript .
22. Jabbari, M. and Dehbani , H., An exact solution for classic coupled othermoporo elasticity in cylinderical coordinate, Journal of Solid Mechanics, 1 (4), 343-357,2009.
23. Kumar,R., and Ailawalia,P., Elastodynamics of inclined loads in micropolar cubic cristal, Mechanics and Mechanical Engineering 9(2), 2005, 57-75,2005.